Original Article

MOLECULAR METABOLISM

Loss of mitochondrial aconitase promotes colorectal cancer progression via SCD1-mediated lipid remodeling

Xin You [1,2,6], Jingyu Tian [1,3,6], Hui Zhang [1,3,6], Yunhua Guo [1,3], Jing Yang [1], Chaofeng Zhu [1], Ming Song [1], Peng Wang [1], Zexian Liu [1], John Cancilla [4], Wenhua Lu [1,3], Christophe Glorieux [1], Shijun Wen [1], Hongli Du [5], Peng Huang [1,3], Yumin Hu [1,3,*]

ABSTRACT

Objective: Mitochondrial aconitase (ACO2) is an essential enzyme that bridges the TCA cycle and lipid metabolism. However, its role in cancer development remains to be elucidated. The metabolic subtype of colorectal cancer (CRC) was recently established. We investigated ACO2's potential role in CRC progression through mediating metabolic alterations.

Methods: We compared the mRNA and protein expression of ACO2 between paired CRC and non-tumor tissues from 353 patients. Correlations between ACO2 levels and clinicopathological features were examined. CRC cell lines with knockdown or overexpression of ACO2 were analyzed for cell proliferation and tumor growth. Metabolomics and stable isotope tracing analyses were used to study the metabolic alterations induced by loss of ACO2.

Results: ACO2 decreased in >50% of CRC samples compared with matched non-tumor tissues. Decreased ACO2 levels correlated with advanced disease stage ($P < 0.001$) and shorter patient survival ($P < 0.001$). Knockdown of ACO2 in CRC cells promoted cell proliferation and tumor formation, while ectopic expression of ACO2 restrained tumor growth. Specifically, blockade of ACO2 caused a reduction in TCA cycle intermediates and suppression of mitochondrial oxidative phosphorylation, resulting in an increase in glycolysis and elevated citrate flux for fatty acid and lipid synthesis. Increased citrate flux induced upregulation of stearoyl-CoA desaturase (SCD1), which enhanced lipid desaturation in ACO2-deficent cells to favor colorectal cancer growth. Pharmacological inhibition of SCD selectively reduced tumor formation of CRC with ACO2 deficiency.

Conclusions: Our study demonstrated that the rewiring metabolic pathway maintains CRC survival during compromised TCA cycles and characterized the therapeutic vulnerability of lipid desaturation in a meaningful subset of CRC with mitochondrial dysfunction.

Keywords Mitochondrial aconitase; Colon cancer; Tricarboxylic acid (TCA) cycle; Lipogenesis; Stearoyl-CoA desaturase

1. INTRODUCTION

Accumulating evidence has suggested a link between abnormalities of TCA cycle enzymes and tumorigenesis. Genetic defects including isocitrate dehydrogenase (IDH), succinate dehydrogenase (SDH), and fumarate hydratase (FH) have been investigated for metabolic enzyme-mediated oncogenesis [1]. Mitochondrial aconitase (ACO2) catalyzes the interconversion of citrate to isocitrate in the second step of the TCA cycle. Six-carbon citrate is exported across the mitochondrial membrane to the cytosol and further converted into oxaloacetate and two-carbon acetyl-CoA, which is the precursor for fatty acid synthesis. As such, ACO2 is an essential enzyme that bridges the TCA cycle and lipid metabolism.

Genetic changes in tumor suppressor genes including APC in 5q, TP53 in 17p, and DPC4/SMAD4 in 18q have been well characterized in colorectal cancer (CRC) [2–4]. In addition to 5q, 17p, and 18q deletions, loss of chromosome 22 is also frequently detected in CRC [5,6]. A genomic sequencing study of 23 CRC patients indicated deletion of the *ACO2* gene located in 22q13 [7]. A proteomic analysis of seven pairs of CRC tissues and adjacent normal mucosa revealed downregulation of ACO2 in CRC [8]. We also previously observed decreased ACO2 expression in gastric cancer [9]. However, the role of ACO2 in tumorigenesis has not been elucidated.

Four transcriptomic consensus molecular subtypes (CMS) of CRC have been established based on characterization of the gene set enrichment

[1]Sun Yat-sen University Cancer Center, State Key Laboratory of Oncology in South China, Collaborative Innovation Center for Cancer Medicine, Guangzhou, Guangdong, 510060, China [2]Department of Oncology, Molecular Oncology Research Institute, The First Affiliated Hospital of Fujian Medical University, Fuzhou 350005, Fujian, China [3]Sun Yat-sen University Metabolomics Center, Guangzhou, Guangdong, 510080, China [4]Scintillon Institute, San Diego, CA 92121, USA [5]School of Biology and Biological Engineering, South China University of Technology, Guangzhou, Guangdong, 510006, China

[6] Jingyu Tian and Hui Zhang contributed equally.

*Corresponding author. Sun Yat-sen University Cancer Center, State Key Laboratory of Oncology in South China, Collaborative Innovation Center for Cancer Medicine, Guangzhou, Guangdong, 510060, China. E-mail: huym@sysucc.org.cn (Y. Hu).

Received December 10, 2020 • Revision received February 27, 2021 • Accepted February 27, 2021 • Available online 3 March 2021

https://doi.org/10.1016/j.molmet.2021.101203

analysis of key biological features [10]. Specifically, 13% of the samples were defined as CMS3 or metabolic subtypes that reflected enrichment of multiple metabolism signatures including fatty acids and lipids. Herein, we used CRC as a model system to characterize the potential role of ACO2 in tumorigenesis through mediating metabolic alterations.

In this study, we reveal that ACO2 levels decreased in >50% CRC samples compared with matched non-tumor tissues and a low expression of ACO2 was significantly associated with shorter survival times. The high-frequency downregulation of ACO2 suggests an important role of metabolic adaptations for CRC cell survival. Herein, we attempted to identify the metabolic alterations that are critical for the growth and survival of CRC cells in metabolic stress induced by ACO2 deficiency. Better understanding of the metabolic machineries of CRC will provide potential therapeutic strategies for treating a meaningful fraction of CRC patients.

2. MATERIALS AND METHODS

2.1. Human subjects and cell lines

Paraffin-embedded CRC tissues of 331 patients were collected from Sun Yat-sen University Cancer Center with informed consent from each subject. No patient in the study received preoperative anti-cancer treatment. The median follow-up time since the time of diagnosis was 51 months (3–125 months). In addition, 22 pairs of CRC and adjacent normal colorectal mucosa specimens were collected for PCR or Western blotting analysis. The study involving human subjects was approved by the Medical Ethics Committee of Sun Yat-sen University Cancer Center. LoVo and HCT116 cells were obtained from American Type Culture Collection (Rockville, MD, USA). The cells were cultured in RPMI-1640 supplemented with 10% FBS.

2.2. Antibodies and reagents

The following antibodies were used for immunoblotting or immunohistochemistry analyses: anti-ACO2 (ab129069), anti-GAPDH(ab181602), anti-beta actin (ab6276), and anti-Ki67 (ab16667) were purchased from Abcam (Cambridge, MA, USA); anti-alpha tubulin (GT114) was obtained from GeneTex (Irvine, CA, USA); anti-SCD1 (2438), anti-FASN (3180), and anti-ACLY (4332) antibodies were purchased from Cell Signaling Technology (Danvers, MA, USA); anti-SLC25A1 (sc-86392) was obtained from Santa Cruz Biotechnology (Dallas, TX, USA); and A939572 (HY-50709) was purchased from MedChemExpress (Monmouth Junction, NJ, USA).

2.3. Generation of CRC cell lines with knockdown or overexpression of ACO2

Short hairpin RNA (shRNA) sequences targeting ACO2 or non-targeting controls (NCs) were inserted into the LV3-pGLV-H1-GFP/puro lentiviral vector (GenePharma, Suzhou, China). Anti-sense sequences for shACO2 were as follows: shACO2 (5′-GCCCAACGAGTACATCCATTA-3′). Human full-length cDNA of ACO2 was cloned into LV5- pGLV-EF1a-GFP/puro lentiviral plasmid vector and designated as oeACO2 (GenePharma, Suzhou, China). The empty vector was used as a negative control. The cells were infected with lentivirus supernatant and selected in medium containing puromycin (2 μg/mL). LoVo cells transfected with LV3-pGLV-H1-GFP/puro lentiviral vector expressing non-targeting and shACO2 sequences are hereafter referred to as LoVo-nc and LoVo-shACO2, respectively.

2.4. Glycolytic activity

Glucose uptake and lactate secretion were measured using a Yellow Springs Instrument 2950D-1 (YSI) Biochemistry Analyzer (YSI Life Sciences, Yellow Springs, OH, USA). Quantification was determined by the difference in substrate concentrations between the final spent medium and initial medium and normalized by the cell number over 24 h.

2.5. Acetyl-CoA and malonyl-CoA levels

Cells from a 6-well plate were extracted with 110 μl of 5% perchloric acid (Sigma–Aldrich). The samples were then centrifuged at 15,000 × *g* (10 min at 4 °C). The supernatant was transferred to a vial and 3 μl was loaded onto a 6495 Triple Quad LC/MS (Agilent, Santa Clara, CA, USA) equipped with a BEH amide column (2.1 mm × 100 mm and 1.7 μm particles, Waters). The transition to quantify Acetyl-CoA is 810 -> 303. The abundance of acetyl-CoA was expressed as peak areas on a mass spectrometer and calculated with Agilent MassHunter Workstation Software. The level of malonyl-CoA was measured by a human malonyl coenzyme A ELISA Kit from CUSABIO as instructed (Cusabio, Houston, TX, USA).

2.6. Seahorse XF extracellular flux analyzer

Seahorse XF Cell Mito Stress and glycolysis stress tests were used to measure mitochondrial oxygen consumption and glycolytic activity as previously described [11]. The dependency of the cells to oxidizing major mitochondrial fuels including glucose, glutamine, and fatty acids was measured by a Mito Fuel Flex test. Briefly, the cells were washed with warmed assay medium (Seahorse XF Base medium supplemented with 1 mM of pyruvate, 2 mM of glutamine, and 10 μM of glucose) and then assay medium was added to the cells to adjust the volume to 500 L for Seahorse XF24 microplates. The cells were incubated in a 37 °C non-CO_2 incubator for 1 h prior to the assay. UK5099 (2 μM, an inhibitor of mitochondrial pyruvate carrier), BPTES (3 μM, an inhibitor of inhibitor of glutaminase), and etomoxir (4 μM, an inhibitor of carnitine palmitoyl-transferase 1A) were used to block the oxidation of glucose, glutamine, and fatty acids, respectively. Fuel dependency was determined by first injecting an inhibitor of the target pathway, followed by inhibition of the two alternative pathways. The dependency data analysis was performed by a Seahorse XF Mito Fuel Flex test report generator. The percentage of dependency on specific fuel was calculated by quantifying the changes in basal OCR after its own inhibition divided by the total changes in OCR after combined inhibition of the three inhibitors. All the assays were performed by a Seahorse XF extracellular flux analyzer (Agilent, Santa Clara, CA, USA).

2.7. Stable isotope tracing analysis of TCA cycle intermediates and quantification of newly synthesized fatty acids

Cells were seeded in a 6-well plate in triplicate wells and cultured overnight. The culture medium was replaced with glucose-free RPMI-1640 medium with 10% FBS supplemented with [U−$^{13}C_6$]-glucose or [U−$^{13}C_5$]-glutamine (>99%; Cambridge Isotope Laboratories). After 24 h, the cells were rinsed with 0.9% (w/v) saline twice and quenched with 500 μl of −20 °C methanol. Then 200 μL of ice-cold water containing 1 μg of norvaline internal standard (Cambridge Isotope Laboratories) was added to the cell lysates and transferred to fresh sample tubes. Then 500 μL of −20 °C chloroform was added to the tubes and extracts were vortexed for 15 min. The samples were centrifuged at 12,000 rpm for 10 min at 4 °C. The top aqueous layer was collected and evaporated in a vacuum centrifuge at 4 °C. Dried intracellular metabolites were kept at −20 °C until derivatization for GC–MS analysis. To interpret labeling patterns, mole percentage enrichment (MPE) of isotopes was calculated as the percent of all atoms within the metabolite pool that were labeled. The percentage of newly synthesized fatty acids underwent isotopomer spectral analysis (ISA) using a 13C metabolic flux analysis (13C-MFA) software tool INCA as previously described [12,13]

2.8. Targeted metabolomics analysis by gas chromatography-mass spectrometry (GC—MS)

The abundance of the TCA cycle, glycolytic pathway intermediates, and fatty acids were analyzed with Thermo Fisher Scientific TRACE 1310. Polar metabolites and fatty acids were extracted with methanol/water/chloroform. The derivatization and GC—MS analysis were performed as previously described [14]. The acquired spectra were analyzed using XCalibur Qual Browser software (Thermo Fisher Scientific). The intensity of intracellular metabolites was normalized by the intensity of internal standard norvaline.

2.9. Lipidomic analysis by liquid chromatography-mass spectrometry (LC-MS)

The samples were extracted from LoVo cells of five biological replicates and distributed into equal parts for analysis. Lipids from cell pellets were extracted with a mixed solution of methanol, water, and chloroform (5:2:5, v/v/v). The lower phase was collected and dried under a nitrogen gas flow. The dried extracts were stored at −20 °C until analysis. The dried extracts were reconstituted in the mixed solution of acetonitrile and water (1:1, v/v). Quality control (QC) samples were freshly prepared by mixing equal amounts of metabolite extracts from the LoVo-nc and LoVo-shACO2 samples. Briefly, 5 μL of metabolite extracts or QC samples was injected into a Dionex Ultimate 3000 chromatographic system by an auto-sampler. A BEH C18 column (100 × 2.1 mm and 1.7um, Waters) was used for chromatography separation with a flow rate of 0.30 mL/min and a column temperature of 40 °C. The column effluent was directly introduced into the electrospray source of a Q Exactive mass spectrometer (Thermo Fisher Scientific). The samples were run in both positive and negative ionization modes and mass spectrometric data on polar metabolites were acquired in the full MS/data-dependent MS2 (DDA) scan mode (100—1500 *m/z*).
Raw data were acquired using Xcalibur 4.1 (Thermo Fisher Scientific) and lipids were identified with 5 ppm mass tolerance by LipidSearch 4 (Thermo Fisher Scientific). Orthogonal partial least squares-discriminant analysis (OPLS-DA) was used to identify the differential metabolites between two groups using SIMCA-P version 14 (Umetrics, Umeå, Sweden). The most significantly altered lipid metabolites (log2fold change > 1 or < -1, $P < 0.05$, VIP > 1) were further analyzed with MetaboAnalyst (Xia Lab, McGill University, Montreal Quebec, Canada, http://www.metaboanalyst.ca) to identify relevant pathways.

2.10. Animal study of subcutaneous xenografts

Animal experiments were performed under the guidelines of the Institutional Animal Care and Use Committee of Sun Yat-sen University Cancer Center. Female BALB/c nude mice of 4—6 weeks old were purchased from Guangdong Animal Experimental Center (Guangzhou, China). The right flanks of the mice were injected subcutaneously with 1.5×10^6 (LoVo) or 1×10^6 (HCT116) CRC cells expressing control vectors shACO2 or oeACO2. At the end point, all mice were sacrificed and tumors were dissected for weight measurement. To evaluate the therapeutic effects of A939572, 2×10^6 LoVo cells expressing control vector or shACO2 were implanted by subcutaneous injection into the left and right dorsal flank of each mouse, respectively. Nine days after cell injection, the mice were randomized and divided into control and treated group (n = 6 for each group). The treatment group received A939572 (i.p., 20 mg/kg daily). The control group was given an equal volume of assisted solvent. Body weight and tumor volumes were measured twice a week. 4 weeks after treatment, the mice were sacrificed and tumors were collected for measurement.

2.11. Statistical analysis

The correlation between ACO2 expression and clinicopathologic features of CRC patients was analyzed by the χ^2 test. The effect of the ACO2 level on CRC patient survival was evaluated using the Kaplan—Meier method and statistical analysis was performed with log-rank tests. The multivariate Cox regression model was used to estimate the hazard ratios of patient survival associated with ACO2 expression. Error bars indicated means ± S.D. An independent Student's t test or two-way ANOVA was performed to analyze the statistical significance between the groups. The data analysis was performed using Prism software (GraphPad, San Diego, CA, USA). $P < 0.05$ were considered statistically significant.

3. RESULTS

3.1. ACO2 was frequently downregulated in colorectal cancer

A quantitative real-time polymerase chain reaction (qRT-PCR) was performed to compare ACO2 expression between tumor and paired non-tumor tissues in 13 CRC cases. Compared with corresponding non-tumor tissues, a decrease in ACO2 was detected in 11 of the 13 CRC cases ($P = 0.0234$, Figure 1A). The downregulation of ACO2 messenger RNA (mRNA) in CRC was validated in the paired tumors and adjacent normal samples in Cancer Genome Atlas (TCGA) cohorts (n = 50; $P < 0.0001$) (Figure 1B). A similar trend was observed in the unpaired CRC (n = 647) and adjacent normal (n = 51) samples ($P < 0.0001$, Figure 1C). Decreased ACO2 mRNA expression was also detected in multiple CRC cohorts (Supplementary Table S1). Western blotting analysis also showed that ACO2 expression was markedly downregulated in most CRC cases compared with non-tumor counterparts (Figure 1D). Expression of ACO2 was further investigated by IHC in 331 pairs (tumor vs matched non-tumor tissues) of CRC. Representative IHC showed intense staining of ACO2 in the normal tissues and marginally detectable staining in the CRC tissues (Figure 1E). The staining score confirmed that ACO2 decreased at the protein level (Figure 1F, n = 331, $P < 0.0001$). Although deletion of the *ACO2* gene in chromosome 22q has been previously reported [7], to investigate other possibility that may contribute to the frequent downregulation in CRC, we performed a methylation analysis of colorectal adenocarcinoma (COAD) from TCGA. As shown in Supplementary Fig. S1, the methylation level of ACO2 in colorectal cancer was significantly higher than in normal adjacent samples ($P = 6e\text{-}10$), indicating that the *ACO2* gene was hypermethylated.

3.2. ACO2 downregulation was associated with poor CRC prognosis

Statistical analysis of 331 CRC IHC samples revealed that ACO2 expression significantly correlated with the clinical stage ($P < 0.001$), tumor-node metastasis stage (TNM, $P < 0.001$), and pathological differentiation ($P = 0.002$) (Supplementary Table S2). Representative staining images of ACO2 in patients with different stages and differentiations are shown in Supplementary Fig. S2. A Kaplan—Meier survival analysis and log-rank test demonstrated that a low level of ACO2 correlated with shorter overall survival (n = 331, $P < 0.0001$, Figure 1G). The results were consistent with the survival analysis from the TCGA cohort (n = 613, $P = 0.0281$, Figure 1H). Further multivariate COX proportional hazard regression analysis demonstrated that low expression of ACO2 was an independent prognostic factor for shorter disease-specific survival ($P < 0.001$; hazard ratio, 0.420; 95% CI, 0.269—0.656, Supplementary Table S3).

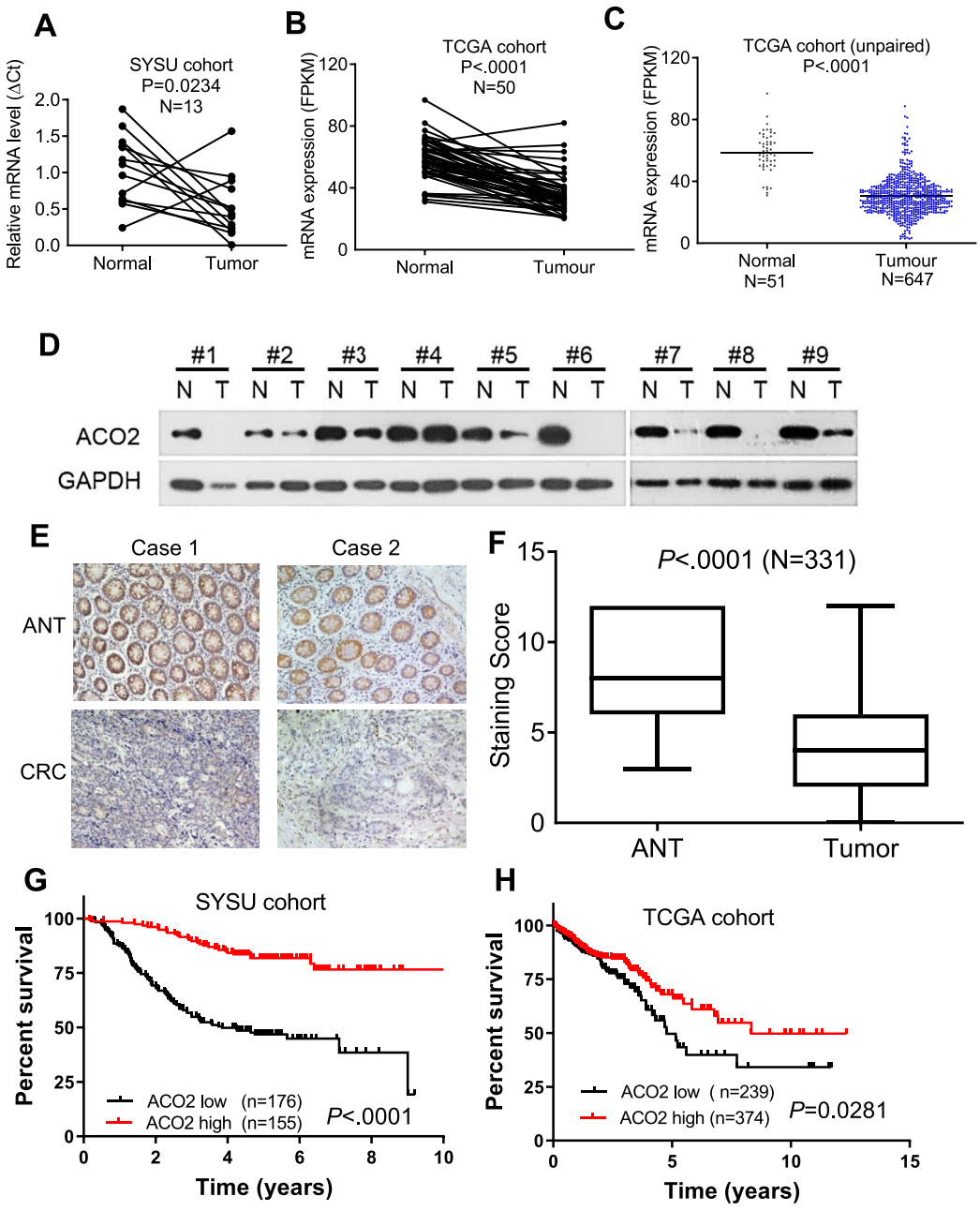

Figure 1: Decreased expression of ACO2 was frequently detected and associated with poor patient outcomes in colorectal cancer (CRC). (A) Reverse transcription PCR showed that ACO2 mRNA was downregulated in CRC tissues compared with normal tissues in the Sun Yat-sen University Cancer Center (SYSU, paired) and (B—C) the Cancer Genome Atlas (TCGA, paired and unpaired) cohorts. FPKM, fragments per kilobase of transcript per million mapped reads. (D) Western blotting analysis of nine specimens from CRC patients showed that ACO2 protein expression was frequently downregulated in CRC tissues (T) compared with adjacent normal tissues (N). (E) Representative immunohistochemistry (IHC) images showing ACO2 staining in CRC tissues and adjacent normal tissues (ANT). Magnification, 200×. (F) Staining intensity of IHC was compared between tumor and corresponding non-tumor tissues ($P < 0.001$, n = 331). (G—H) Low expression of ACO2 protein (SYSU cohort, $P < 0.0001$) and mRNA (TCGA cohort, $P = 0.0281$) was associated with shorter survival in CRC patients.

3.3. Knockdown of ACO2 promoted cell proliferation and tumor formation of CRC

We next evaluated the effect of ACO2 deficiency on CRC cell lines. Endogenous ACO2 was inhibited by shRNAs in LoVo and HCT116 cells. Stable knockdown of ACO2 was verified by a Western blotting analysis (Figure 2A). Inhibition of ACO2 enhanced cell growth and colony formation in CRC cells (Figure 2B). Knockdown of ACO2 in LoVo and HCT116 promoted tumor growth by 36—78% ($P < 0.001$) in subcutaneous xenografts and increased the tumor weight by 18—85% (Figure 2C—D). Ki-67 staining of LoVo-derived tumors also indicated

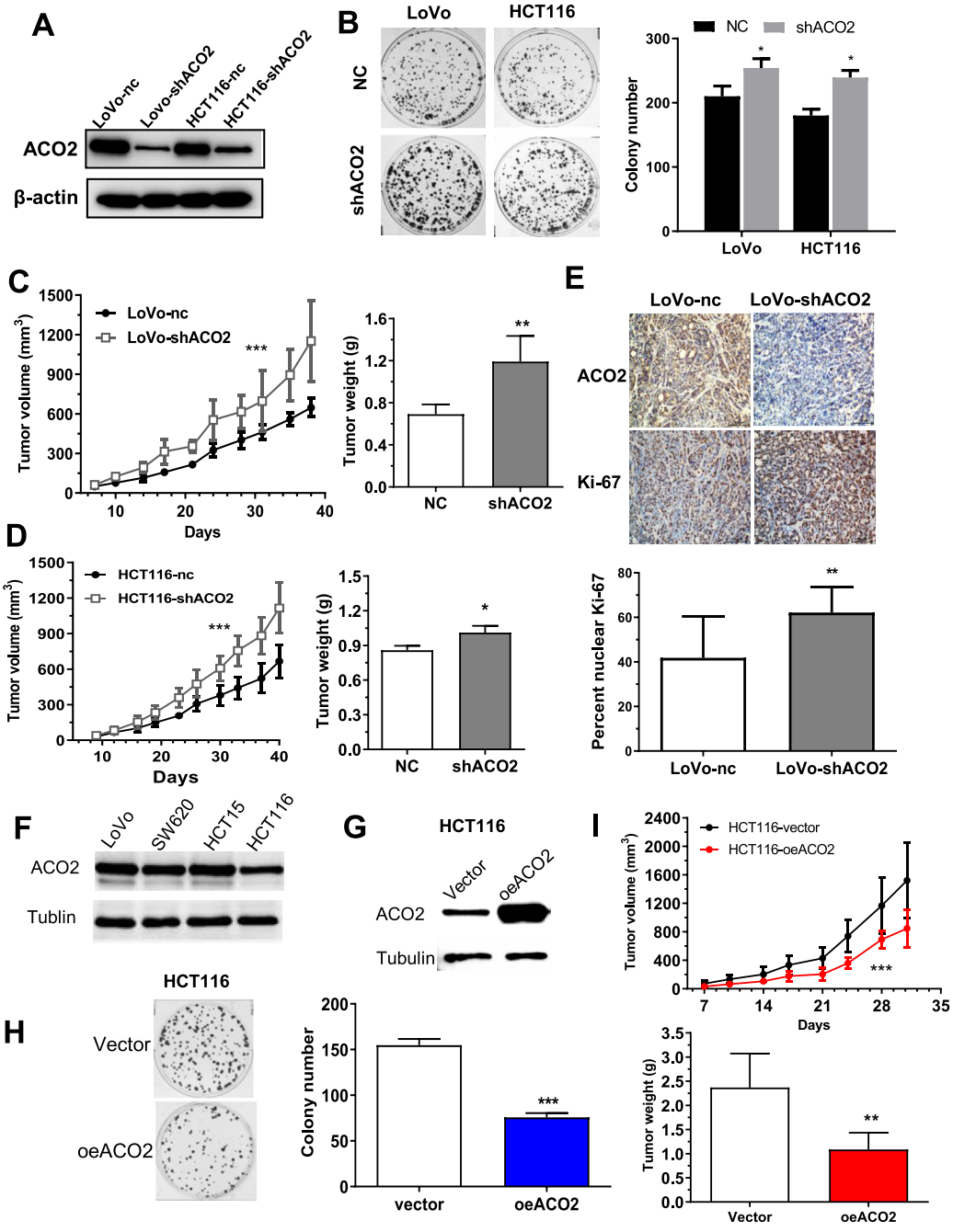

Figure 2: Knockdown of ACO2 promoted cell proliferation and tumor formation in CRC. (A) Knockdown of ACO2 by shRNA was detected in LoVo and HCT116 cells by Western blotting analysis. (B) Knockdown of ACO2 enhanced colony formation in LoVo and HCT116 cells. (C—D) LoVo and HCT116 cells stably expressing shACO2 exhibited accelerated tumor growth compared to control cells expressing non-targeting shRNA (nc). (E) ACO2 knockdown LoVo tumors showed increased cell proliferation as demonstrated by Ki-67 staining. (F) Expression of ACO2 in different CRC cells. (G—I) Ectopic expression of ACO2 in HCT116 cells attenuated colony formation and tumor growth in HCT116 cells. HCT116 vector (transfected with vector control), HCT116-oeACO2 (transfected with plasmid containing ACO2), oeACO2, and ACO2 overexpression. Bars, means ± SD.*$P < 0.05$, **$P < 0.01$, and ***$P < 0.001$.

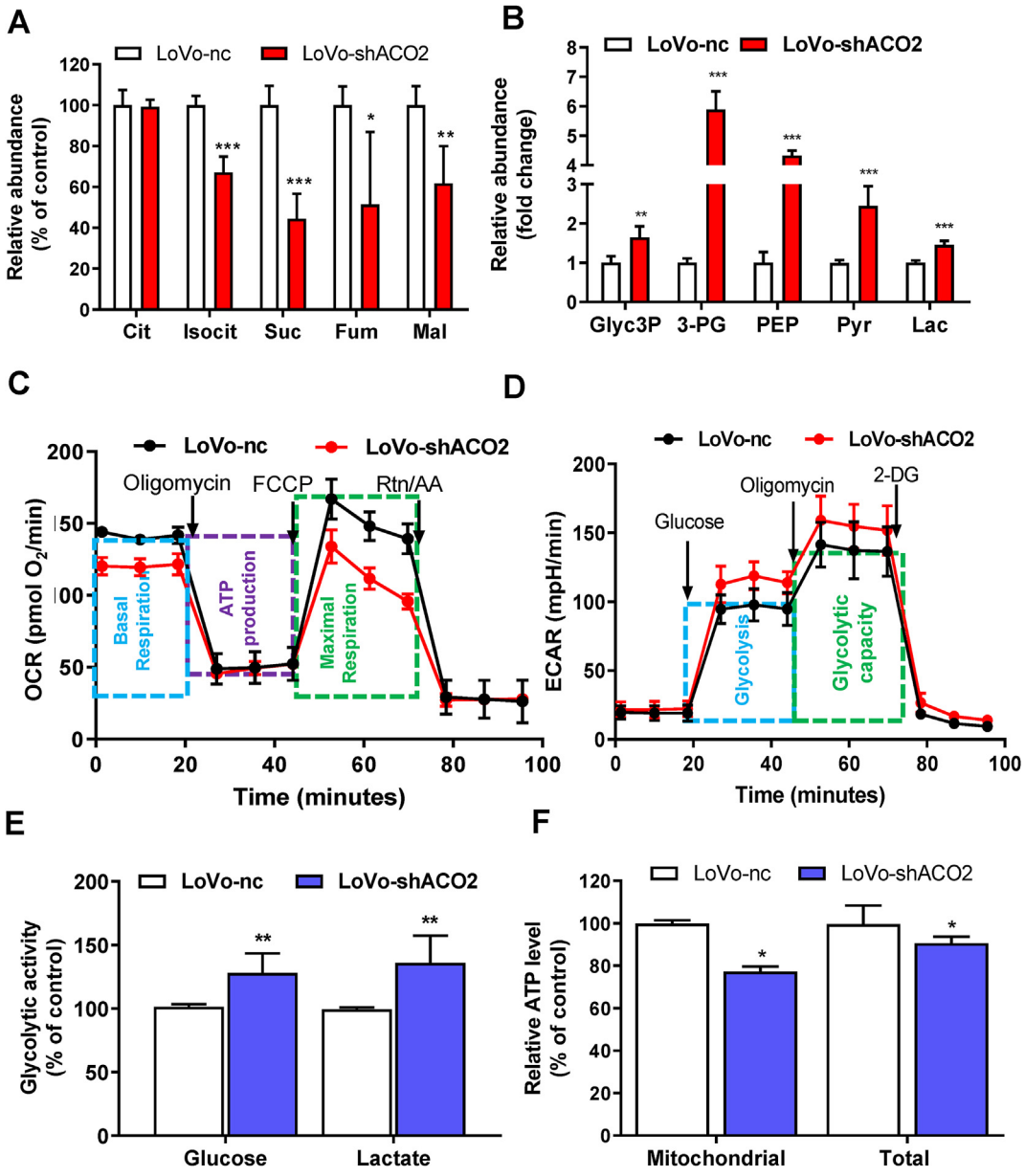

Figure 3: Knockdown of ACO2 perturbed the TCA cycle and promoted glycolytic activity. (A) LoVo cells stably expressing non-targeting shRNA control (nc) and shACO2 were analyzed by gas chromatography-mass spectrometry (GC–MS) for TCA cycle metabolites including citrate (cit), isocitrate (Isocit), succinate (Suc), fumarate (Fum), and malate (Mal). (B) GC–MS analysis for glycolytic intermediates including glycerol 3-phosphate (Glyc3P), 3-phosphoglyceric acid (3-PG), phosphoenolpyruvate (PEP), pyruvate (Pyr), and lactate (Lac). (C) The oxygen consumption rate (OCR, indicator of mitochondrial OXPHOS function) was detected in LoVo-nc and LoVo-shACO2 cells by a Seahorse XF extracellular flux analysis. Compounds including oligomycin, FCCP, rotenone, and antimycin A (Rtn/AA) were injected sequentially at different time points as indicated. Basal respiration (difference between top and bottom blue dashed lines), ATP production (difference between top and bottom purple dashed lines), and maximal respiration (difference between top and bottom green dashed lines). (D) Glycolytic activity was monitored by the extra cellular acidification rate (ECAR) using a Seahorse XF extracellular flux analysis. The compounds including glucose, oligomycin A, and 2-DG were injected sequentially at different time points as indicated. Glycolysis (difference between top and bottom blue dashed lines) and glycolytic capacity (difference between top and bottom green dashed lines). (E) Glucose uptake and lactate production in LoVo-nc and LoVo-shACO2 cells (F), mitochondria-derived ATP, and total ATP production in LoVo-nc and LoVo-shACO2 cells. Bars, means ± SD.*$P < 0.05$, **$P < 0.01$, and ***$P < 0.001$.

cell proliferation promoted by knockdown of ACO2 (Figure 2E). We next examined the effect of ACO2 overexpression on cell growth. Due to the relatively low expression (Figure 2F), we ectopically expressed ACO2 in HCT116 cells (Figure 2G). Overexpression of ACO2 significantly inhibited colony formation in HCT116 cells ($P < 0.001$) (Figure 2H). In contrast to the knockdown effect *in vivo*, overexpression of ACO2 significantly suppressed the growth of HCT116 xenografts in nude mice (Figure 2I).

3.4. Loss of ACO2 caused suppression of oxidative phosphorylation and activation of glycolytic activity

Because ACO2 catalyzes the isomerization of citrate to isocitrate in the TCA cycle, we reasoned that the impaired ACO2 activity perturbed the flow of TCA cycle intermediates and therefore inhibits the electron transport chain (ETC) coupled with oxidative phosphorylation (OXPHOS). First, we performed targeted metabolomics with a gas chromatography-mass spectrometry analysis and demonstrated that

LoVo cells stably expressing shACO2 showed significantly reduced levels of TCA cycle intermediates, including isocitrate, succinate, fumarate, and malate (Figure 3A). Moreover, ACO2 knockdown caused a significant increase in glycolysis intermediates including glycerol 3-phosphate, phosphoenolpyruvate, 3-phosphoglyceric acid, pyruvate, and lactate (Figure 3B).

Seahorse XF analysis was then used to evaluate the activity of OXPHOS (oxygen consumption rate, OCR) and glycolysis (extracellular acidification rate, ECAR), which are the two major energy-producing pathways in cells. We observed attenuated mitochondrial OXPHOS coupled with increased glycolytic activity in LoVo cells after ACO2 knockdown (Figure 3C—D). Moreover, we found that compared with LoVo-nc cells, LoVo-shACO2 cells exhibited higher glucose uptake coupled with elevated levels of lactate production (Figure 3E). The attenuated mitochondrial OXPHOS and increase in glycolysis was also confirmed in HCT116 and HCT15 cells with ACO2 knockdown (Supplementary Fig. S3). Calculation from OCR demonstrated that ATP production from mitochondria decreased by approximately 25% in the ACO2 knockdown cells. However, we observed an approximately 10% decrease in total ATP levels after ACO2 knockdown (Figure 3F). Our data indicated that glycolysis was the compensatory pathway for energy supply when mitochondrial oxidative phosphorylation was compromised.

3.5. Glutamine oxidation maintained the TCA cycle for citrate formation upon loss of ACO2

Because glucose and glutamine are two major substrates to support energy production and macromolecular synthesis for cell survival [12,13], colorectal cancer cell proliferation with dysfunctional oxidative phosphorylation prompted us to further investigate the metabolic route of the TCA cycle with ACO2 deficiency. We first compared the oxidation of glucose and glutamine using a Mito Fuel Flex test (Figure 4A). Three inhibitors of major fuel pathways including UK5099 (mitochondrial pyruvate carrier), BPTES (glutaminase), and etomoxir (palmitoyltransferase 1A) were used to test the reliance on specific metabolites to maintain baseline respiration. We found that glucose and glutamine consisted of approximately 30% of the total fuel oxidation in LoVo cells, respectively. However, glucose oxidation decreased to 20% and glutamine oxidation increased to 38% after ACO2 knockdown, indicating the activation of the glutaminolysis pathway. To further characterize the metabolic routes, we cultured the LoVo cells with [U—13C]-glucose or [U—13C]-glutamine and examined the carbon source as demonstrated by the atom transition map shown in Figure 4B. The TCA intermediates including succinate, fumarate, malate, and citrate labeled with [U—13C]-glucose (M+2) decreased after ACO2 knockdown (Figure 4C). In contrast, the [U—13C]-glutamine (M + 4) contribution to the metabolites significantly increased (Figure 4D). These data collectively indicated that blockade of ACO2 prevented glucose flow and activated anaplerosis from glutamine oxidation in the TCA cycle. To further characterized the alteration of glutamine metabolism in the TCA cycle after ACO2 knockdown, we measured both the oxidative metabolism and reductive carboxylation of [U—13C]-glutamine. As shown in Figure 4E, oxidative metabolism generated pyruvate and alanine with three 13C (M + 3), aspartate, and citrate with four 13C (M + 4), while reductive carboxylation generated aspartate with three 13C (M + 3) and citrate with five 13C (M + 5). Loss of ACO2 caused a significant increase in the metabolites that flow from glutamine oxidation including pyruvate (M + 3), alanine (M + 3), aspartate (M + 4), and citrate (M + 4). In contrast, no significant alterations of aspartate (M+3) or citrate (M+5) were detected (Figure 4F). Overall, our data demonstrated the critical role of glutamine-dependent anaplerosis to maintain the TCA cycle and produce citrate upon loss of ACO2.

3.6. Knockdown of ACO2 enhanced fatty acid synthesis and β-oxidation via acetyl-CoA accumulation

Fatty acids are energy-rich compounds and their acyl group can be transferred to carnitine. Acylcarnitine is then transported into the mitochondria for repeated rounds of oxidation and hydration. This process is known as β-oxidation [15]. We reasoned that ACO2 deficiency may direct citrate flux into the cytosol for acetyl-CoA pools, thus promoting fatty acid synthesis. We indeed found a significant increase in acetyl-CoA, newly synthesized palmitate (14%—26%), and stearate (10%—14%) after ACO2 knockdown (Figure 5A—B). Consistently, we found increased palmitoylcarnitine (fold change = 3.1, $P < 0.05$), acetylcarnitine (fold change = 3.3, $P < 0.001$), and hexanoylcarnitine (fold change = 21.2, $P < 0.01$) in ACO2 knockdown cells (Figure 5C). We only observed a marginal increase in carnitine in CRC cells with ACO2 knockdown (fold change = 1.196, $P < 0.01$), which along with a higher level of carnitine derivatives may suggest enhanced transport of fatty acids through mitochondrial membranes. Fatty acid synthesis also involves interconversion of acetyl-coA and malonyl-CoA, which is a critical regulator of β-oxidation by inhibiting carnitine acyltransferase such as CPT [16]. Therefore, decreased malonyl-coA levels after ACO2 knockdown may also contribute to enhanced β-oxidation by releasing the inhibition of CPT (Figure 5D). The accumulation of acetyl-coA and elevated fatty acid levels prompted us to evaluate the oxidation of fatty acids. The ratio of fatty acid oxidation to the total fuel oxidation substantially enhanced after knockdown of ACO2 in LoVo cells (4.4-fold increase, $P < 0.01$) (Figure 5E). Taken together, our findings suggested that upregulation of *de novo* fatty acid synthesis from acetyl-CoA along with reduced inhibition of carnitine palmitoyltransferase (CPT) by malonyl-CoA promoted mitochondrial-driven oxidation under metabolically stressed conditions induced by loss of ACO2 (Figure 5F).

3.7. CRC cells exhibited enhanced lipogenesis and lipid unsaturation upon loss of ACO2

Fatty acid synthesis is required to synthesize new membrane rafts and store energy in lipid droplets for highly proliferative cancer cells [17]. We performed a global lipidomic analysis using liquid chromatography-tandem mass spectrometry (LC-MS/MS) to determine the effect of loss of ACO2 on lipid metabolism. The samples were extracted from LoVo cells of five biological replicates and distributed into equal parts for analysis. The OPLS-DA analysis revealed that LoVo-shACO2 cells had a specific group of metabolites that was different from LoVo cells (Supplementary Fig. S4A). Moreover, a differential analysis showed a total of 799 altered lipids after knockdown of ACO2 (log2fold change > 1 or < -1, $P < 0.05$) (Supplementary Fig. S4B). The altered lipids were then analyzed with MetaboAnalyst to identify relevant metabolic pathways. According to the *P* and impact values, the most significant altered pathways were related to metabolism of glycerophospholipids and sphingolipids (Supplementary Fig. S4C), which constitute the key structural lipids in cell membranes [18]. The quantitative analysis further demonstrated that loss of ACO2 was closely associated with increased levels of glycerophospholipids including phosphatidylcholine (PC, fold change = 1.3, $P < 0.01$), phosphatidylethanolamine (PE, fold change = 1.4, $P < 0.01$), phosphatidylinositol (PI, fold change = 1.3, $P < 0.001$), phosphatidylserine (PS, fold change = 1.3, $P < 0.01$), cardiolipin (CL, fold change = 2.2, $P < 0.001$), and sphingolipids including ceramide (Cer, fold change = 2.4, $P < 0.001$) and sphingomyelin (SM, fold change = 1.6, $P < 0.001$) (Figure 6A). Interestingly, we found reduced levels of

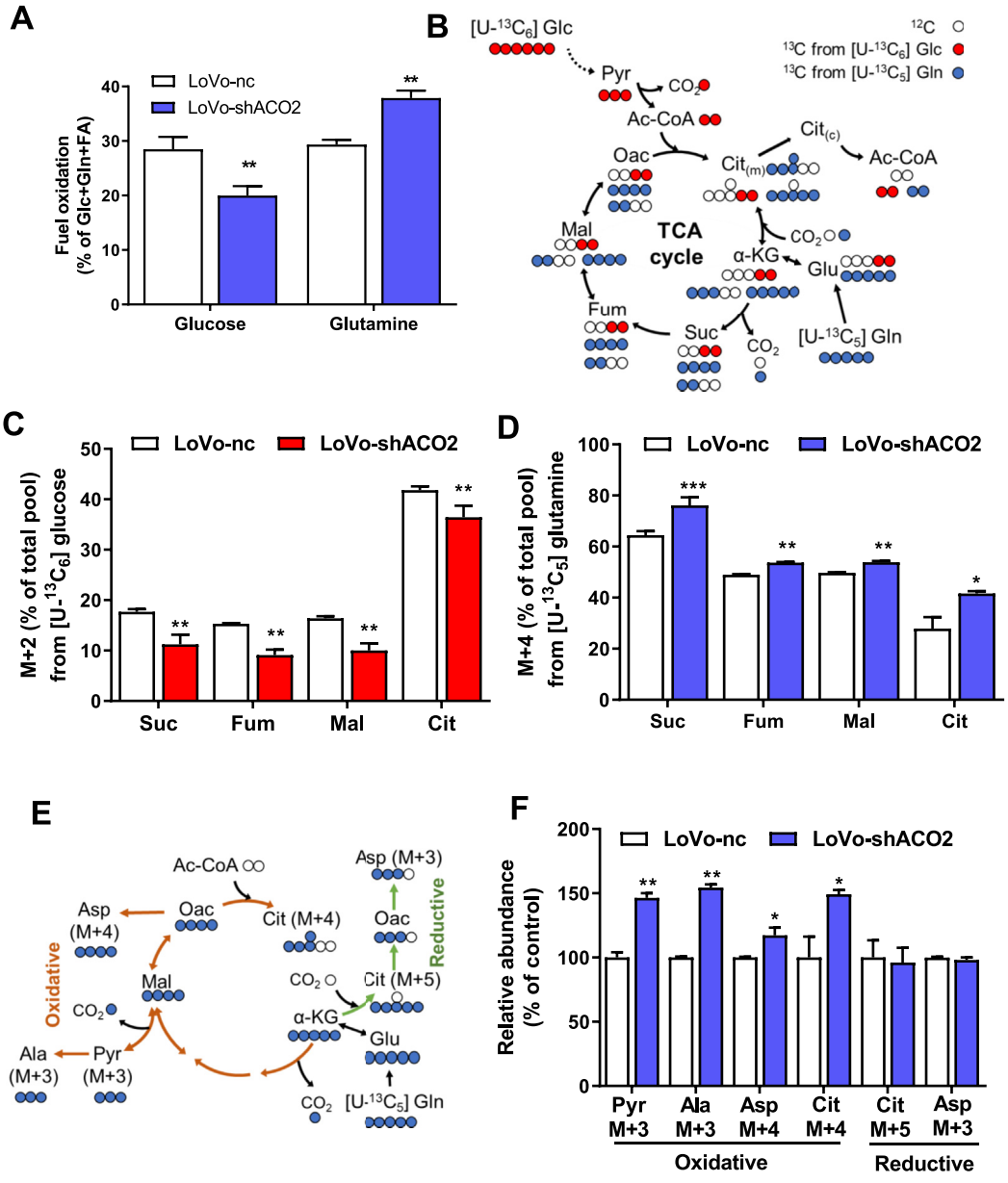

Figure 4: Increased glutamine oxidation supported citrate production upon loss of ACO2. (A) Contribution of glucose and glutamine to mitochondrial oxidation before and after ACO2 knockdown was measured by a Seahorse XF Mito Fuel Flex test. (B) Schematic depicting citrate and acetyl-coA production from glucose and glutamine metabolism in the TCA cycle. Red circles and green circles represent ^{13}C atoms derived from [U−^{13}C]-glucose and [U−^{13}C]-glutamine, respectively. Open circles represent ^{12}C atoms. Dashed lines indicate multi-step atomic transitions. Cit(m), mitochondrial citrate. Cit(c), cytosolic citrate. Ac-CoA, acetyl-CoA; αKG, α-ketoglutarate; Cit, citrate; Fum, fumarate; Glc, glucose; Glu, glutamate; Gln, glutamine; Mal, malate; Oac, oxaloacetate; Pyr, pyruvate; Suc, succinate. (C−D) Contribution of glucose and glutamine carbon to TCA cycle intermediates as measured by mole percent enrichment from [U−^{13}C]-glucose (M+2) and [U−^{13}C]-glutamine (M+4) after culturing LoVo cells for 24 h with the isotopes. (E) Schematic routes of anaplerosis supply and reductive carboxylation of [U−^{13}C]-glutamine. Orange and green arrows indicate oxidative and reductive glutamine metabolism in the TCA cycle, respectively. (F) Mass isotopolog level of intermediates from oxidative and reductive metabolism after culturing LoVo cells for 24 h with [U−^{13}C] glutamine. Bars, means ± SD. $*P < 0.05$, $**P < 0.01$, and $***P < 0.001$.

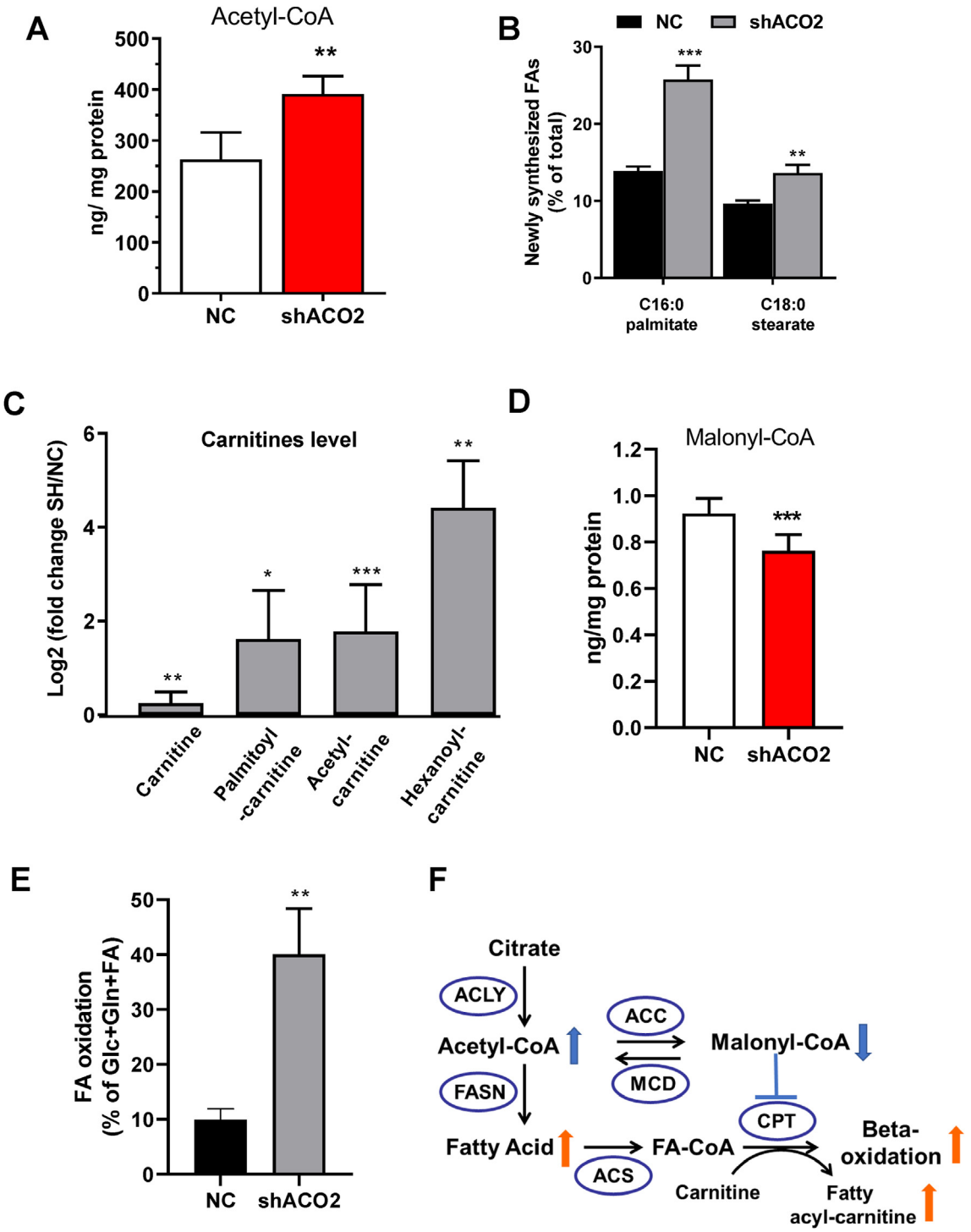

Figure 5: Loss of ACO2 promoted fatty acid synthesis and β oxidation. (A) Enhanced acetyl-CoA accumulation in LoVo cells after ACO2 knockdown. (B) Increased percentage of newly synthesized fatty acids compared to the total amount of fatty acids in LoVo cells after ACO2 knockdown. (C) Fold changes of carnitine and derivatives were calculated by the average level of the ACO2 knockdown (SH) cells compared to control cells (NC). (D) Decreased Malonyl-CoA concentrations in LoVo cells after ACO2 knockdown. (E) The contribution of fatty acid to mitochondrial oxidation before and after ACO2 knockdown was measured by a Seahorse XF Mito Fuel Flex test. (F) Schematic diagram summarizing the alteration in fatty acid oxidation upon loss of ACO2 in CRC cells. Knockdown of ACO2 promoted citrate flux to acetyl-CoA production and subsequent fatty acid synthesis. Decreased flow to malonyl-CoA releases suppression on CPT (carnitine palmitoyltransferase). Upregulation of fatty acyl-carnitine further promoted beta oxidation. ACLY, ATP citrate lyase; FASN, fatty acid synthase; ACC, acetyl-CoA carboxylase; MCD, malonyl-CoA decarboxylase; ACS, acetyl-CoA synthetase; CPT, carnitine palmitoyltransferase. Bars, means ± SD.*$P < 0.05$, **$P < 0.01$, and ***$P < 0.001$.

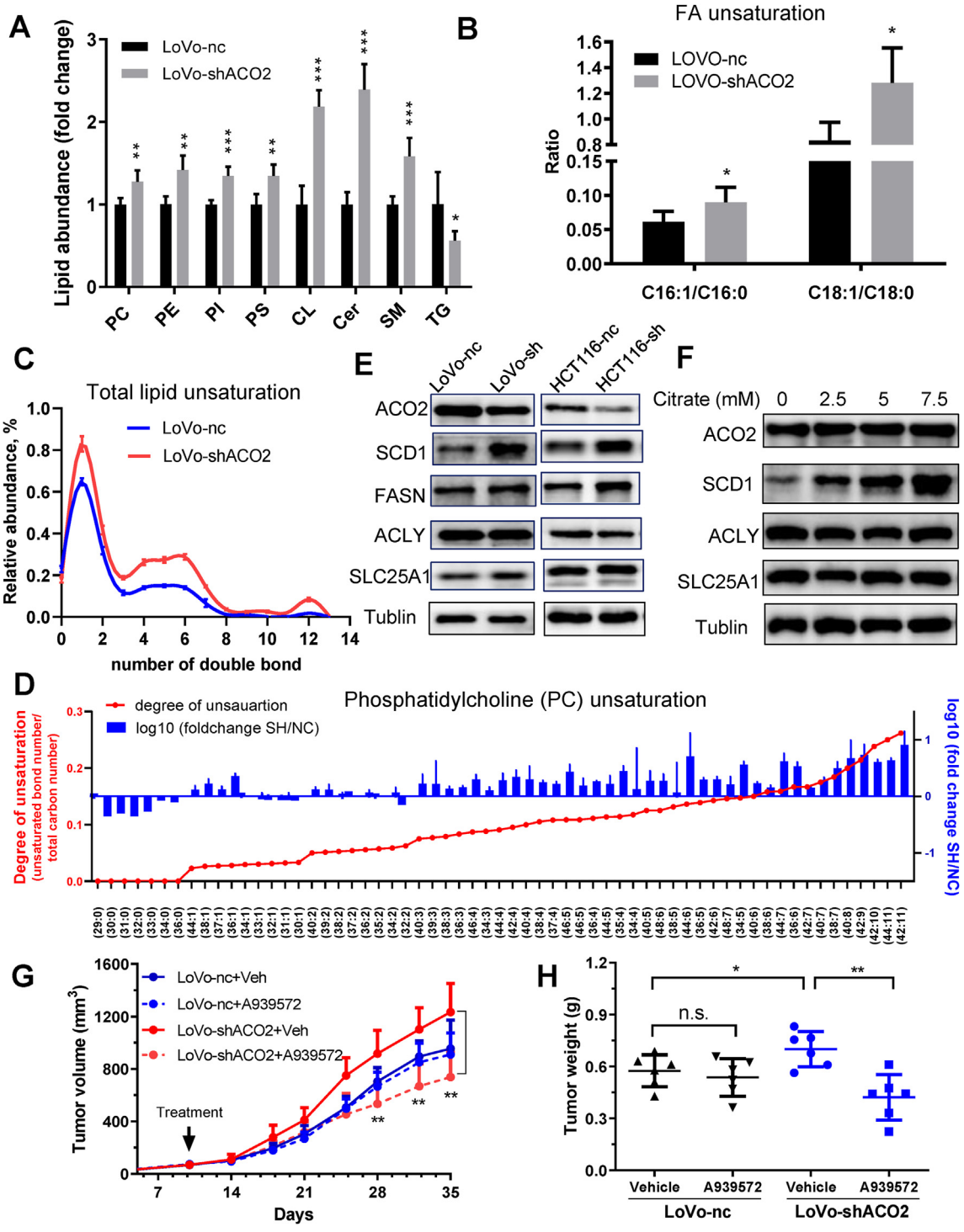

Figure 6: Knockdown of ACO2 induced SCD1 expression and enhanced lipid unsaturation. (A) Glycerophospholipid including phosphatidylcholine (PC), phosphatidylethanolamine (PE), phosphatidylinositol (PI), phosphatidylserine (PS), cardiolipin (CL), and sphingolipids including ceramide (Cer) and sphingomyelin (SM) increased upon knockdown of ACO2. The triglyceride (TG) level was reduced after ACO2 knockdown in LoVo cells. (B) Quantitation of the ratios of unsaturated FAs to saturated FAs in the ACO2 knockdown cells and control cells. (C) Total lipid unsaturation in LoVo-nc and LoVo-shACO2 cells (n = 5). The unsaturation degree was calculated using the average lipid level divided by the number of lipid compounds with the indicated double bonds. (D) Individual PC species was shown as number of double bonds (0–11) divided by length of FA side chains (carbons: C29 to C42). The red line indicates the degree of unsaturation. Fold change was calculated using the mean level of specific lipid species in LoVo-shACO2 compared to LoVo-nc (Sh/NC) (E) Western blotting analysis of ACO2, SCD1, FASN, ACLY, and SLC25A1 in CRC cells before and after ACO2 knockdown with actin as a loading control. (F) Western blotting analysis of LoVo cells before and after treatment with citrate at various concentrations for 72 h. Treatment of citrate caused an elevated expression of SCD1. The expression of ACLY and SLC25A1 was not affected. (G–H) Subcutaneous tumor volume and final weight of LoVo-nc and LoVo-shACO2 cells treated with vehicle control (Veh) or A939572 (n = 6 tumors per group). Bars, means ± SD.*$P < 0.05$, **$P < 0.01$, and ***$P < 0.001$.

triglycerides (TG) in LoVo-shACO2 cells (fold change = 0.5, $P < 0.05$). Because TGs are stored in lipid droplets, we reasoned that loss of ACO2 may activate lipolysis and release of free fatty acids.

One important modification of the biophysical properties of lipids is the number of double bonds in the acyl chain [19]. We next examined the lipid composition (saturated vs unsaturated bonds) after ACO2 knockdown. As shown in Figure 6B, the ratio of unsaturated fatty acids (16:1 and 18:1) to saturated fatty acids (16:0 and 18:0) significantly increased after ACO2 knockdown in LoVo cells. The levels of the measured unsaturated bonds (1−13) unanimously increased in LoVo-shACO2 cells (Figure 6C). The FA composition was also analyzed in PC, a major lipid class that constitutes structural membranes and shows rapid turnover of acyl chains [18,20]. A large variety of PC molecules with different lengths and saturation of FA side chains was detected in LoVo cells. As shown in Figure 6D, the individual PC clusters are demonstrated as the number of double bonds (0−11) divided by the length of the FA side chains (carbons C29 to C42), indicating the unsaturation level. Importantly, a substantial increase in unsaturated PC species containing one or more double bonds was detected in LoVo-shACO2 compared to LoVo-nc cells.

3.8. Inhibition of lipid desaturase selectively suppressed tumor growth of CRC with ACO2 deficiency

To determine the source of unsaturated lipids in the ACO2 knockdown cells, we examined the level of metabolic enzymes involved in lipogenesis including citrate transport protein (SLC25A1), ATP-citrate lyase (ACLY), fatty acid synthase (FASN), and stearoyl-CoA desaturase (SCD1). SCD1 catalyzes the synthesis of monounsaturated fatty acids, palmitoleate (16:1), and oleate (18:1) from palmitate (16:0) and stearate (18:0), respectively [21]. We showed a significant increase in the ratio of unsaturated FA to saturated FA in the ACO2 knockdown cells (Figure 6B). Importantly, the immunoblotting analysis revealed markedly enhanced SCD1 expression upon loss of ACO2 in CRC cells (LoVo, HCT116), while no significant change was detected in other enzymes (Figure 6E) such as FASN, ACLY, and SLC25A1. Given that the citrate:isocitrate ratio is upregulated in ACO2-dificient cells, we next evaluated whether supplementation of citrate may affect the expression of SCD. We found that treating LoVo cells with exogenous citrate for 72 h upregulated SCD1 in a dose-dependent manner. Consistently, no detectable change was observed in other major enzymes in the lipogenesis pathway (Figure 6F). We also showed that citrate supplementation caused a significant increase in intracellular acetyl-CoA levels and concomitant upregulation of acetyl-histone H3 (Supplementary Fig. S5). Our data suggested that loss of ACO2 may promote SCD1 expression through histone acetylation. A939572, a small molecule inhibitor that specifically targets SCD1 enzymatic activity [22,23], was then used to test the functional significance of lipid desaturation to cell survival of CRC cells with ACO2 deficiency. The MTS assay demonstrated that A939572 effectively reduced the cell viability of the ACO2 knockdown cells, whereas the LoVo-nc cells were less sensitive (Supplementary Fig. S6). We tested whether inhibition of desaturase impaired tumor formation of CRC cells with loss of ACO2. We transplanted LoVo cells subcutaneously into immunodeficient mice. We found that LoVo-nc-derived tumors exhibited no response to A939572 treatment. In contrast, A939572 significantly decreased growth rates and final weights of LoVo-shACO2-derived tumors (Figure 6G−H). Our data suggested that inhibition of lipid desaturation selectively suppressed CRC cell growth under metabolic stress induced by loss of ACO2.

4. DISCUSSION

Mitochondrial aconitase (ACO2) is an essential TCA cycle enzyme that catalyzes the reversible isomerization of citrate to isocitrate. In this study, we demonstrated that ACO2 was frequently downregulated in CRC tissues and lower expression significantly correlated with poor differentiation ($P = 0.002$) and advanced clinical stage ($P < 0.001$). ACO2 knockdown promoted CRC cell growth *in vitro* and tumorigenicity *in vivo*. In contrast, ectopic expression of ACO2 significantly inhibited CRC cell proliferation. These findings together indicate that loss of ACO2 may favor the malignant phenotype of CRC. How CRC cells survive potential metabolic stress upon repression of ACO2 activity remains to be elucidated.

Our results demonstrated that CRC cells activated metabolic adaptations to enhance survival under stress induced by loss of ACO2. We first observed perturbed TCA cycle metabolism with attenuated oxidative phosphorylation (OXPHOS). Consistent with our data, previous studies with paired colon cancer tissue and normal tissue showed that intermediates of the TCA cycle were downregulated in cancer compared to normal counterparts [24]. Moreover, we found that glycolytic activity was activated while glucose entry to the TCA cycle for oxidation became limited. However, glutamine and fatty acid oxidation were significantly upregulated to maintain the TCA cycle and OXPHOS. Importantly, stable isotope tracing analysis revealed increased glutamine-derived carbon and reduced glucose carbon contribution to TCA cycle intermediates. Therefore, blockade of ACO2 hindered the oxidative metabolism of glucose carbon and activate glutamine supply for anaplerosis in the TCA cycle. Indeed, knockdown of ACO2 caused elevated glutamine-derived citrate and decreased glucose-derived citrate in CRC cells.

Citrate is a critical TCA cycle intermediate for subsequent cascade of fatty acid synthesis. Decreased ACO2 expression presumably causes higher levels of citrate. We observed an increased ratio of citrate/isocitrate, although no significant accumulation of citrate was detected after ACO2 knockdown in the CRC cells. We reasoned that limiting ACO2 activity may have caused a redirection of citrate to the cytosol and lead to rapid turnover for *de novo* synthesis of fatty acids. We indeed observed a perturbed TCA cycle metabolism with attenuated oxidative phosphorylation and increased production of fatty acids. Consistent with our data, previous studies with paired colon cancer tissue and normal tissue showed that intermediates of the TCA cycle were downregulated in cancer compared to that in normal counterparts [24]. Moreover, the upregulation of glycolysis and fatty acid oxidation contributed a considerable fraction of the energy supply in CRC cells with defective mitochondria caused by loss of ACO2.

Importantly, we demonstrated that loss of ACO2 induced major alterations in lipid metabolism characterized by enhanced lipid abundance and unsaturation. Of note, previous studies showed that the cytosolic pool of acetyl-CoA is also supplied by the ligation of acetate and CoA by acetyl-CoA synthetase (ACSS), which contributes to FA synthesis and maintains breast and prostate cancer cell growth under serum-deprived or hypoxic conditions [25]. The role of acetate in the contribution to FA synthesis in the context of CRC with ACO2 deficiency is worth further investigation.

Furthermore, the lipidomic analysis demonstrated that glycerophospholipid was the most significantly altered pathway in the ACO2 knockdown cells. Of note, over-enrichment of multiple metabolism signatures including glucose, glutamine, fatty acid, and glycerophospholipid was found in consensus molecular subtype 3 (CMS3) of CRC [10], which was consistent with the metabolic alterations observed in this study. Beyond its effect on lipid synthesis, we uncovered the enhanced lipid unsaturation caused by ACO2 knockdown

in CRC cells. The ACO2 knockdown cells exhibited a higher ratio of unsaturated fatty acids to saturated fatty acids (16C and 18C) compared with the control cells. The conversion of saturated fatty acid to monounsaturated fatty acid is known to be mediated by SCD1 [19,26], which was upregulated in the ACO2 knockdown cells in this study. Therefore, upregulation of SCD may be crucial for membrane synthesis to compensate for the defect of mitochondrial metabolism in CRC cells with ACO2 deficiency. Of note, a recently defined CRC gene signature suggests that SCD is overexpressed in stage II CRC patients with a high risk of relapse [27]. We demonstrated that pharmacological inhibition of SCD selectively suppressed the *in vivo* growth of CRC with ACO2 knockdown. Thus, the metabolic requirement for lipid unsaturation in ACO2-deficient CRC presents a therapeutic vulnerability.

5. CONCLUSIONS

The perturbation of the TCA cycle and attenuated OXPHOS induced by loss of ACO2 provide direct evidence of dysfunctional mitochondria in colorectal cancer. Our study highlights the metabolomic roadmap of metabolic rewiring to override stress induced by ACO2 deficiency. For the first time, we report that decreasing ACO2 enhances fatty acid synthesis and lipid desaturation, leading to a lipogenic phenotype to promote CRC growth. Better understanding of the metabolic machineries of CRC will provide potential therapeutic strategies for treating a meaningful fraction of CRC patients.

AUTHOR CONTRIBUTIONS

Conceptualization: Hui Zhang, Peng Huang, and Yumin Hu. Investigation, formal analysis, and methodology: Xin You, Hui Zhang, Jingyu Tian, Yunhua Guo, Jing Yang, Chaofeng Zhu, Ming Song, Zexian Liu, John Cancilla, Wenhua Lu, Christophe Glorieux, Shijun Wen, and Hongli Du. Validation: Xin You and Yumin Hu. Original draft: Xin You and Yumin Hu. Review and editing: Xin You and Yumin Hu. Funding acquisition: Yumin Hu.

CONFLICT OF INTEREST

The authors declare that they have no known competing financial interests or personal relationships that could have appeared to influence the work reported in this paper.

ACKNOWLEDGMENTS

This study was supported by the National Key R&D Program of China (No. 2018YFC0910203), the National Natural Science Foundation of China (No. 81871982), the Natural Science Foundation of Guangdong Province (2018A030313022), the Key R&D Program of Guangdong Province (No. 2019B020226001), and the Project of Education and Scientific Research for Young and Middle-Aged Teachers in Fujian Province (No. JAT190203).

APPENDIX A. SUPPLEMENTARY DATA

Supplementary data to this article can be found online at https://doi.org/10.1016/j.molmet.2021.101203.

REFERENCES

[1] Sajnani, K., Islam, F., Smith, R.A., Gopalan, V., Lam, A.K., 2017. Genetic alterations in Krebs cycle and its impact on cancer pathogenesis. Biochimie 135:164–172.

[2] Vogelstein, B., Fearon, E.R., Hamilton, S.R., Kern, S.E., Preisinger, A.C., Leppert, M., et al., 1988. Genetic alterations during colorectal-tumor development. New England Journal of Medicine 319(9):525–532.

[3] Groden, J., Thliveris, A., Samowitz, W., Carlson, M., Gelbert, L., Albertsen, H., et al., 1991. Identification and characterization of the familial adenomatous polyposis coli gene. Cell 66(3):589–600.

[4] Baker, S.J., Fearon, E.R., Nigro, J.M., Hamilton, S.R., Preisinger, A.C., Jessup, J.M., et al., 1989. Chromosome 17 deletions and p53 gene mutations in colorectal carcinomas. Science 244(4901):217–221.

[5] Yana, I., Kurahashi, H., Nakamori, S., Kameyama, M., Nakamura, T., Takami, M., et al., 1995. Frequent loss of heterozygosity at telomeric loci on 22q in sporadic colorectal cancers. International Journal of Cancer 60(2):174–177.

[6] Zarzour, P., Boelen, L., Luciani, F., Beck, D., Sakthianandeswaren, A., Mouradov, D., et al., 2015. Single nucleotide polymorphism array profiling identifies distinct chromosomal aberration patterns across colorectal adenomas and carcinomas. Genes Chromosomes & Cancer 54(5):303–314.

[7] Laiho, P., Hienonen, T., Mecklin, J.P., Jarvinen, H., Karhu, A., Launonen, V., et al., 2003. Mutation and LOH analysis of ACO2 in colorectal cancer: no evidence of biallelic genetic inactivation. Journal of Medical Genetics 40(5):e73.

[8] Bi, X., Lin, Q., Foo, T.W., Joshi, S., You, T., Shen, H.M., et al., 2006. Proteomic analysis of colorectal cancer reveals alterations in metabolic pathways: mechanism of tumorigenesis. Molecular & Cellular Proteomics 5(6):1119–1130.

[9] Wang, P., Mai, C., Wei, Y.L., Zhao, J.J., Hu, Y.M., Zeng, Z.L., et al., 2013. Decreased expression of the mitochondrial metabolic enzyme aconitase (ACO2) is associated with poor prognosis in gastric cancer. Medical Oncology 30(2):552.

[10] Guinney, J., Dienstmann, R., Wang, X., de Reynies, A., Schlicker, A., Soneson, C., et al., 2015. The consensus molecular subtypes of colorectal cancer. Nat Med 21(11):1350–1356.

[11] Huang, A., Ju, H.Q., Liu, K., Zhan, G., Liu, D., Wen, S., et al., 2016. Metabolic alterations and drug sensitivity of tyrosine kinase inhibitor resistant leukemia cells with a FLT3/ITD mutation. Cancer Letters 377(2):149–157.

[12] Young, J.D., 2014. INCA: a computational platform for isotopically nonstationary metabolic flux analysis. Bioinformatics 30(9):1333–1335.

[13] Antoniewicz, M.R., 2018. A guide to (13)C metabolic flux analysis for the cancer biologist. Experimental & Molecular Medicine 50(4):19.

[14] Zhang, H., Badur, M.G., Divakaruni, A.S., Parker, S.J., Jager, C., Hiller, K., et al., 2016. Distinct metabolic states can support self-renewal and lipogenesis in human pluripotent stem cells under different culture conditions. Cell Reports 16(6):1536–1547.

[15] Rohrig, F., Schulze, A., 2016. The multifaceted roles of fatty acid synthesis in cancer. Nature Reviews Cancer 16(11):732–749.

[16] Foster, D.W., 2012. Malonyl-CoA: the regulator of fatty acid synthesis and oxidation. Journal of Clinical Investigation 122(6):1958–1959.

[17] Currie, E., Schulze, A., Zechner, R., Walther, T.C., Farese Jr., R.V., 2013. Cellular fatty acid metabolism and cancer. Cell Metabolism 18(2):153–161.

[18] Beloribi-Djefaflia, S., Vasseur, S., Guillaumond, F., 2016. Lipid metabolic reprogramming in cancer cells. Oncogenesis 5:e189.

[19] Peck, B., Schulze, A., 2016. Lipid desaturation - the next step in targeting lipogenesis in cancer? FEBS Journal 283(15):2767–2778.

[20] Peck, B., Schug, Z.T., Zhang, Q., Dankworth, B., Jones, D.T., Smethurst, E., et al., 2016. Inhibition of fatty acid desaturation is detrimental to cancer cell survival in metabolically compromised environments. Cancer & Metabolism 4:6.

[21] Nakamura, M.T., Nara, T.Y., 2004. Structure, function, and dietary regulation of delta6, delta5, and delta9 desaturases. Annual Review of Nutrition 24:345–376.

[22] Xin, Z., Zhao, H., Serby, M.D., Liu, B., Liu, M., Szczepankiewicz, B.G., et al., 2008. Discovery of piperidine-aryl urea-based stearoyl-CoA desaturase 1 inhibitors. Bioorganic & Medicinal Chemistry Letters 18(15):4298–4302.

[23] von Roemeling, C.A., Marlow, L.A., Wei, J.J., Cooper, S.J., Caulfield, T.R., Wu, K., et al., 2013. Stearoyl-CoA desaturase 1 is a novel molecular

therapeutic target for clear cell renal cell carcinoma. Clinical Cancer Research 19(9):2368–2380.

[24] Denkert, C., Budczies, J., Weichert, W., Wohlgemuth, G., Scholz, M., Kind, T., et al., 2008. Metabolite profiling of human colon carcinoma–deregulation of TCA cycle and amino acid turnover. Molecular Cancer 7:72.

[25] Schug, Z.T., Peck, B., Jones, D.T., Zhang, Q., Grosskurth, S., Alam, I.S., et al., 2015. Acetyl-CoA synthetase 2 promotes acetate utilization and maintains cancer cell growth under metabolic stress. Cancer Cell 27(1):57–71.

[26] Fritz, V., Benfodda, Z., Rodier, G., Henriquet, C., Iborra, F., Avances, C., et al., 2010. Abrogation of de novo lipogenesis by stearoyl-CoA desaturase 1 inhibition interferes with oncogenic signaling and blocks prostate cancer progression in mice. Molecular Cancer Therapeutics 9(6):1740–1754.

[27] Vargas, T., Moreno-Rubio, J., Herranz, J., Cejas, P., Molina, S., Gonzalez-Vallinas, M., et al., 2015. ColoLipidGene: signature of lipid metabolism-related genes to predict prognosis in stage-II colon cancer patients. Oncotarget 6(9): 7348–7363.

